Development of a Second Order Dynamic Stall Model

Niels Adema[1], Menno Kloosterman[2], Gerard Schepers[1]

[1]EUREC European Master in Renewable Energy, Hanze University of Applied Sciences, Groningen, 9747 AS, The Netherlands

[2]DNV GL, Groningen, 9743 AN, The Netherlands

*Correspondence to*: Adema N.C. Niels (nielsadema1994@gmail.com)

Abstract. Dynamic stall phenomena bring risk for negative damping and instability in wind turbine blades. It is crucial to model these phenomena accurately to reduce inaccuracies in predicting design driving (fatigue and extreme) loads. Some of the inaccuracies in current dynamic stall models may be due to the facts that they are not properly designed for high angles of attack, and that they do not specifically describe vortex shedding behaviour. The Snel second order dynamic stall model attempts to explicitly model unsteady vortex shedding. This model could therefore be a valuable addition to a turbine design software such as Bladed. In this paper the model has been validated with oscillating airfoil experiments and improvements have been proposed for reducing inaccuracies. The proposed changes led to an overall reduction in error between the model and experimental data. Furthermore the vibration frequency prediction improved significantly. The improved model has been implemented in Bladed and tested against small scale turbine experiments at parked conditions. At high angles of attack the model looks promising for reducing mismatches between predicated and measured (fatigue and extreme) loading. Leading to possible lower safety factors for design and more cost efficient designs for future wind turbines.

1. Introduction

Wind turbines operate in highly unsteady aerodynamic environments (Leishman, 2002). For design and certification, design load cases (DLC's) have been set which describe the conditions that wind turbine designs have to withstand (DNV GL, 2016). Some of the design driving DLC's are those for parked and idling conditions where wind turbine blades will experience high angles of attack (AoA), leading to (dynamic) stall behaviour (Schreck et al., 2000). The wind turbine yaw angle is defined as the angle in the horizontal plane between the free stream wind direction and the wind turbine rotor shaft. It can be noted that when the turbine is parked, and the blades pitched to 90°, the yaw angle effectively becomes the inflow angle. When the yaw system is not operating during parked conditions due to a failure, the blades will experience flow from all direction. For particular wind directions the flow on the blades is separated leading to dynamic stall effects. These effect may already appear at inflow angles of below 30 and 20 degrees (Gonzalez and Munduate, 2007). Therefore, accurate modelling of dynamic stall is therefore crucial in wind turbine design (Choudry et al., 2014).

Dynamic stall is a phenomenon leading to larger variations in lift, drag and pitching moments on the airfoil than would be observed during steady operation (Choudry et al., 2014). This, in case, creates larger aerodynamic forces on the blades than

expected during steady condition (Leishman, 2002). Dynamic stall happens with dynamic variation of the inflow and/or the effective angle of attack and can be viewed as a delay in the onset of stall. Recirculation of flow after the static stall angle starts near the trailing edge and rapidly moves towards the leading edge. Leading to the formation of a large dynamic stall clockwise vortex at the leading edge at increasing angles of attack. The dynamic stall vortex will travel along the suction side from the leading towards the trailing edge before detaching completely. Full separation will occur when the dynamic stall vortex is completely detached. This moment is called the 'break' or 'dynamic stall onset'. As result, low lift remains until re-attachment of the flow. However, a time delay for reattachment of the flow is present as well. After reattachment the process repeats creating a hysteresis loop. Dynamic stall phenomena bring risk for negative damping and instability. Especially if the airfoil is oscillating in and out of stall (McCroskey, 1981). A visual description for dynamic stall is presented in figure (1).
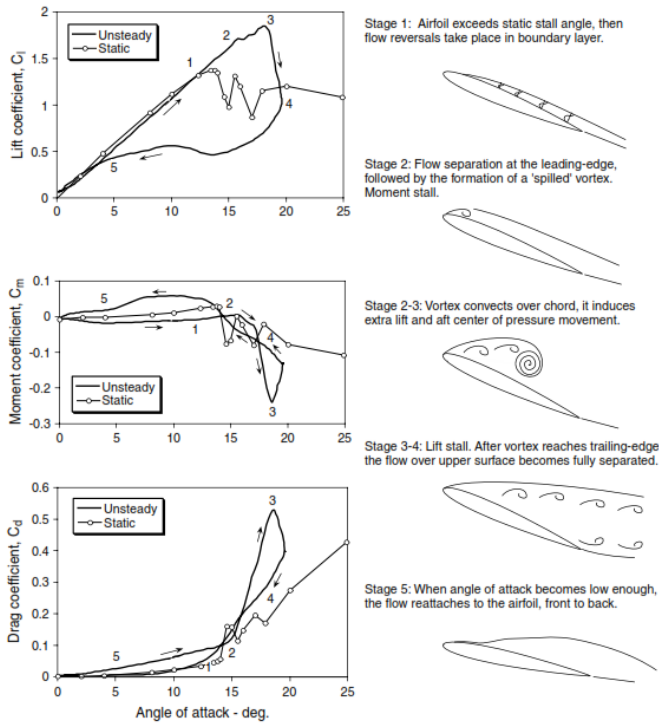
Figure 1: Classical Visual Representation of Dynamic Stall (Leishman, 2002)

When keeping the airfoil pitched in (deep) stall for longer periods of time, periodic vortex shedding will occur. No longer a single large dynamic stall vortex will be shed but multiple periodic vortices from both the leading and trailing edge. This will induce time varying loads on the blades (Riziotis et al., 2010). The periodic vortex shedding is characterised by the Strouhal number representing the dimensionless frequency of shedding (Pellegrino and Meskell, 2013). The Strouhal number is defined following Eq. (1):

$$St = \frac{f * c}{U},$$
(1)

In which f notes the characteristic vortex shedding frequency, c the airfoil chord (sometimes the projected chord length perpendicular to the incoming flow), and U the wind velocity at the wind turbine blade section. Synchronization of the natural and Strouhal frequencies (a "lock-in") will lead to resonance (Pellegrino and Meskell, 2013). Locked-in vortex induced vibrations are a potential threat in standstill conditions as the turbine size is increasing. Modern aeroelastic tools with dynamic stall models are only able to provide accurate deep stall loads at conditions close to maximal lift, so relative small angles of attack (Riziotis et al., 2010). The same study noted that today's aeroelastic tools are not properly tuned for high angles of attack. Mismatches between load predictions between measurements and engineering tools have found to be as high as 20% for high wind speed dynamic stall conditions (Schreck, 2002). State of the art aerodynamic models overestimate fatigue loading with 15% (Schepers and Snel, 2007). (Madsen et al., 2019) shows promise for using Computation Fluid Dynamics (CFD) in early stages of wind turbine design and shape optimization and (Sørensen et al., 2016) showed that CFD models had good agreement with instrumented rotor experiments. So although CFD is becoming more available and useful in wind turbine design it requires large computational power, therefore these tools are not yet fit for practical design calculations. In the industry there is a need for relatively fast and accurate engineering models predicting key loading. (Hollierhoek et al. 2013) studied different dynamic stall models namely: Beddoes Leishman, ONERA, and Snel. However, a clear single best model was not found. (Gonzalez and Munduate, 2007) and (Wala, et al. 2018) both showed promising results using modified and optimized Beddoes Leishman models against experimental data. Inaccuracies in dynamic stall models may be due to the above described facts that they are not properly designed for high angles of attack, and that there are some of them that do not specifically describe vortex shedding behaviour. The Snel second order dynamic stall model does attempt to explicitly model unsteady vortex shedding. However, a need for further tuning and validation of the model is still required (Snel 1997). Snel takes the model from (Truong, 1993) as starting point. (Truong, 1997) already showed promise by modifying his model for unsteady vortex shedding and Snel takes a similar approach. However, as described in chapter 2, the Snel model differs from the Truong model by incorporating the steady lift coefficient and is therefore interesting to study and modify. This paper will provide a detailed analysis into the Snel second order model and will try to answer the following main research question:

What are possible ways to improve predictions of blade vibrations during dynamic stall in parked conditions using the Snel second order model?

This paper will have the following outline:

- The Snel model is validated against experimental data.
- Proposed changes are presented based on the validation results to improve the model predictions. These include a dimensional analysis, calculation of the slope for the potential lift coefficient, application of the normal force coefficient, an investigation into the downstroke and vortex shedding predictions of the model, and finally an optimization for empirical constants.
- Attention will be paid to vibration prediction as this influences turbine fatigue loading which has a large impact on the design of the wind turbine.
- An absolute error analysis is carried out before and after the improvements to quantify the increase in performance.

- The improved model will be tested with actual small scale turbine experimental data to assess performance in combination with Bladed.

2. Analysis and Validation of the Snel Second Order Model

85   This chapter will validate the Snel model and propose adaptations to the model to improve the performance. The description of the model is based on the description in both (Snel, 1993) and (Hollierhoek et al., 2013). (Snel, 1997) derived a dynamic stall model based on the work of (Truong, 1993) who proposed that the dynamic lift coefficient can be distinguished in two parts namely Δc_{l1} and Δc_{l2}:

$$c_{l,dyn} = c_{l,steady} + \Delta c_{l1} + \Delta c_{l2} \,, \tag{2}$$

90   The first describes the forcing frequency response and the second term the self-exited higher frequency dynamics. Snel follows this approach but also expresses the first part as the difference from the steady state (time averaged) lift coefficient (Montgomerie, 1996). The dynamic lift of the Snel model will be as in Eq. (2). The first part, Δc_{l1}, must decay to zero when no excitation is present while the second part will decay to zero for small angles of attack, but nearing stall the second part will show periodic oscillations related to vortex shedding.

95   In the original model of Truong the first part is based on the Beddoes-Leishman dynamic stall model. The Snel model uses the SIMPLE (Montgomerie, 1996) as a departure point for the first order correction while (Truong, 1993) uses the B-L model to calculate Δc_{l1}. The modelling of the first part will therefore follow:

$$\tau \Delta \dot{c}_{l1} + cf_{10} \Delta c_{l1} = ft_1 \,, \tag{3}$$

The forcing term ft_1 will be based on the time derivative of the difference between the steady and potential lift coefficient.
100   This is shown in Eq. (4) and (5). The function is made non-dimensional by taking the coefficient of the derivative term as the time constant usually used in dynamic stall. This constant is described in Eq. (11).

$$ft_1 = \tau \Delta \dot{c}_{l,pot} \,, \tag{4}$$

$$\Delta c_{l,pot} = c_{l,pot} - c_{l,steady} = 2\pi \sin(\alpha - \alpha_0) - c_{l,steady} \,, \tag{5}$$

The coefficient of Δc_{l1} can be seen as a spring trying to pull the term back to the steady state. The stiffness of the spring of
105   this equation is given by Eq. (6). In downwards pitching motion the stiffness is higher than in upwards pitching motion.

$$cf_{10} = \begin{cases} \dfrac{1+0.5\Delta c_{l,pot}}{8(1+60\tau\dot{\alpha})} & if \ \dot{\alpha} c_{l,pot} \leq 0 \\[2mm] \dfrac{1+0.5\Delta c_{l,pot}}{8(1+80\tau\dot{\alpha})} & if \ \dot{\alpha} c_{l,pot} > 0 \end{cases} \,, \tag{6}$$

The second part of the dynamic lift coefficient is of second order to create the higher frequency dynamics. This will be a non-linear mass-damper-spring system following:

$$\tau^2 \Delta \ddot{c}_{l2} + cf_{21} \Delta \dot{c}_{l2} + cf_{20} \Delta c_{l2} = ft_2 \,, \tag{7}$$

110   The spring and damping coefficients are taken from (Snel, 1997) and are defined as in Eq. (8) and (9) respectively.

$$cf_{20} = k_s^2 \left[1 + 3\left(\Delta c_{l2}\right)^2\right]\left[1 + 3\dot{\alpha}^2\right],$$

(8)

$$cf_{21} = \begin{cases} 60\tau k_s \left[-0.01\left(\Delta c_{l,pot} - 0.5\right) + 2\left(\Delta c_{l2}\right)^2\right] & if\ \dot{\alpha} > 0 \\ 2\tau k_s & if\ \dot{\alpha} \leq 0 \end{cases},$$

(9)

Also here it can be noted that the response will be different in pitching upwards or downwards. The forcing term is defined as:

$$ft_2 = 0.1k_s\left(-0.15\Delta c_{l,pot} + 0.05\Delta \dot{c}_{l,pot}\right),$$

(10)

115   In the second order part of the model k_s is taken as the reduced vortex shedding frequency or Strouhal number. This is given a value of 0.2 as in the original model (Snel, 1997) In the above equations the time constant is given below and can be seen as the time it takes for the wind to travel half a chord distance:

$$\tau = c/2U,$$

(11)

2.1 Initial Model Implementation and Validation

120   The Snel model as described in the section above is implemented in a MATLAB environment. The numerical implementation follows the steps described in (de Vaal, 2009). The timestep used is 0.001 seconds to capture higher frequency events from the Ohio State University experiments. The Ohio State University (OSU) experiments (Hoffmann et al., 1996) will be used for validation of the initial implementation of the Snel model. In the OSU experiments an extensive set of airfoils have been tested for both unsteady and steady data. The measurements recorded responses to forced sinusoidal pitching oscillations. Different

125   amplitudes, mean angles of attack, oscillation frequencies and Reynolds numbers were tested. The focus in this paper will be on the NACA4415 and S809 Airfoils. The model parameters obtained from the OSU database, as displayed in table (1), will be analyzed. The oscillation frequencies of the cases are set such that the forcing angle of attack matches the OSU experiments. Figures (2) and (3) show the time series of the lift coefficient for cases with both low and high reduced frequencies, low and high mean angles of attack. The following observations can been made for the current model:

130   -   The current model over predicts the loss of lift during the downstroke.

  -   The predicted vortex shedding does not always happen at the correct time.

  -   There is currently no unsteady vortex shedding at higher angles of attack.

  -   The shedding frequency is not dependent on the reduced frequency while the experiments do show a dependency.

These points will be analysed as part of the possible improvements described in chapters 3.3 up to 3.9.

135

140

Airfoil	# Test Case	Mean wind Speed [m/s]	Average Angle of Attack [deg]	Amplitude [deg]	Oscillation Frequency [Hz]
S809	1	42.8	8.1	10.2	0.60
	2	43.0	8.2	10.1	1.20
	3	42.7	8.3	10.2	1.89
	4	42.8	13.2	10.4	0.60
	5	41.7	12.9	10.1	1.22
	6	42.0	12.9	10.1	1.81
	7	42.3	18.8	10.2	0.61
	8	42.1	18.8	10.1	1.18
	9	42.6	18.7	10.0	1.84
NACA 4415	11	37.9	7.0	11.2	0.61
	12	37.9	7.5	10.8	1.20
	13	37.8	7.3	10.7	1.85
	14	37.8	14.0	10.5	0.60
	15	37.7	14.1	10.6	1.22
	16	37.3	14.1	10.6	1.81
	17	37.2	18.6	10.5	0.61
	18	37.1	18.3	10.8	1.24
	19	37.2	18.4	10.7	1.84

Table 1: Selected cases from the OSU Experiments
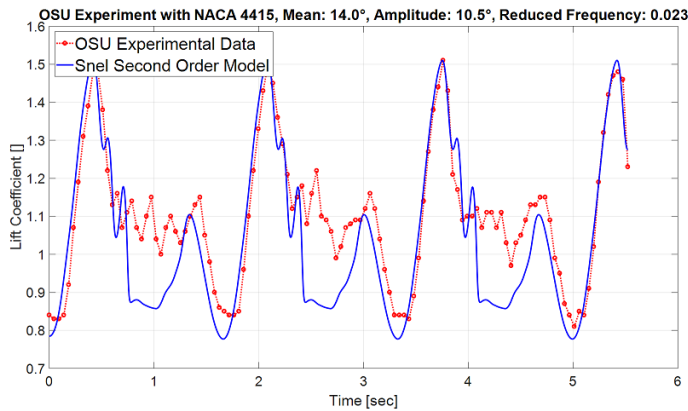
Figure 2: Lift coefficient time of the initial Snel model (NACA 4415 Airfoil with mean angle of attack of 14°, amplitude of 10.5°, and reduced frequency of 0.023)
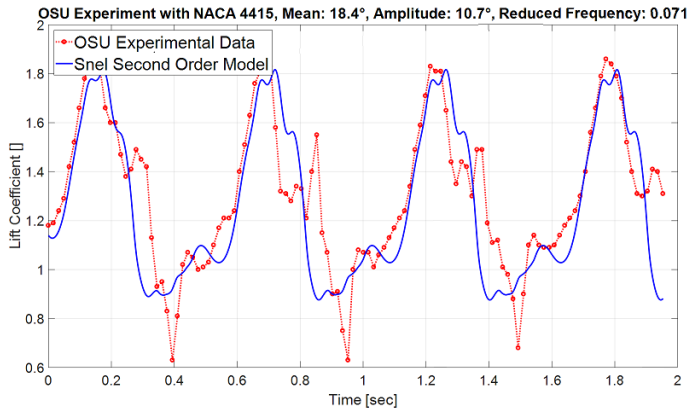
Figure 3: Lift coefficient time of the initial Snel model (NACA 4415 Airfoil with mean angle of attack of 18.4°, amplitude of 10.7° and reduced frequency of 0.071)

2.2 Error Analysis

To quantify the accuracy of the Snel model, the total absolute error between model predictions and experimental data is calculated. This will give an objective measure to assess proposed improvements. The Snel model is interpolated along the Angle of Attack to obtain the dynamic lift coefficient output at the precise angles of attack of the OSU Experiment. The errors are then evaluated according to:

$$E_i = c_{l,model}(\alpha_i) - c_{l,OSU}(\alpha_i),$$
(12)

And the total absolute error of all datapoints is calculated using:

$$Absolute\ Error = \sqrt{\frac{1}{n} \sum_{i=1}^{n} E_i^2},$$
(13)

In which n denotes the number of datapoint of the OSU experimental data

3. Proposed Changes to the Snel Model

This chapter will outline proposed modifications to the Snel model. The following areas will be investigated for modification:

- A dimensional analysis of the model
- The calculation method of the slope for the potential lift coefficient
- Application of the normal force coefficient instead of the lift force coefficient
- The Downstroke prediction of the model is investigated
- Prediction of vortex shedding
- And lastly an optimization for empirical (airfoil specific) constants

7

3.1 Dimensional Analysis

It can be seen in the formulation of the model that Eq. (8) and (10) are cast in a dimensional form. For different values for chords, wind speed and pitching frequency the current model will not produce identical results. In order to make them dimensionless, the time constant used in dynamic stall (Eq. (11)) is added. The new constants will be such that the initial value of the constant is kept. The equations will now be:

$$cf_{20} = k_s^2[1 + 3(\Delta c_{l2})^2][1 + 280^2\tau^2\dot{\alpha}^2], \tag{14}$$

$$ft_2 = 0.1k_s(-0.15\Delta c_{l,pot} + 8\tau\Delta\dot{c}_{l,pot}), \tag{15}$$

3.2 Correct Slope for Cl potential

The Snel model uses 2π as theoretical slope for lift coefficient at low angles of attack. This theoretical value might not be applicable to real airfoils. Calculating the precise slope improves the accuracy of the model. Therefore the slope calculated from the airfoil polar is used in the model. The slope is calculated between the intercept at angle of attack = 0 and the intercept at lift coefficient = 0.

3.3 Application of the Normal Force Coefficient

The Snel model uses the lift coefficient of the steady airfoil data. However, the lift coefficient tends to zero when angles of attack reach 90°. At 90° angle of attack there is still unsteady vortex shedding present. Therefore, it would make sense to model vortex shedding to the normal force on the airfoil instead of the lift force. The normal force coefficient together with the lift and drag coefficients are presented in figure 4. For implementation all the C_L terms are change to C_n terms. A couple of additions must then be made to the model to obtain the dynamic lift and drag coefficients. First, the steady normal force coefficient ($c_{n,steady}$) is the sum of the steady lift and drag coefficient and the angle of attack following:

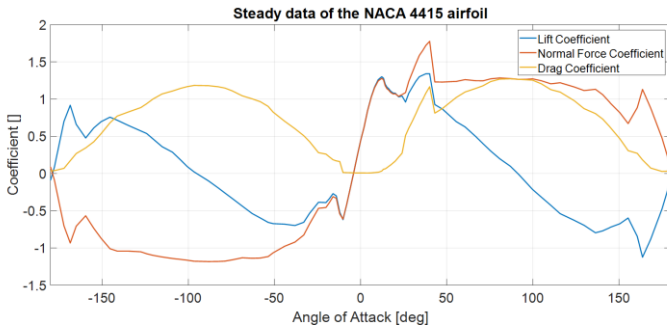$$c_{n,steady} = c_{l,steady}\cos(\alpha) + c_{d,steady}\sin(\alpha), \tag{16}$$

and the steady chordwise coefficient ($c_{c,steady}$) will follow:

$$c_{c,steady} = -c_{l,steady}\sin(\alpha) + c_{d,steady}\cos(\alpha), \tag{17}$$

When the dynamic normal force coefficient has been obtained an inverse calculation yields the lift and drag coefficients:

$$c_{l,dyn} = c_{n,dyn}\cos(\alpha) - C_{c,steady}\sin(\alpha), \tag{18}$$

$$c_{d,dyn} = c_{n,dyn}\sin(\alpha) + C_{c,steady}\cos(\alpha), \tag{19}$$

Figure 4: Steady Polars of the NACA 4415 Airfoil

3.4 Downstroke of the Model

The consistent differences between the implementation of the Snel second order model and earlier implementations are lower values in the downstroke. Figure (5) shows the first and second order part of the model as function of time. The second order part (Δc_{l2}) contributes highly to the lower values at the start of the downstroke which causes a large part of the observed error. Eq. (10) uses $-0.15\Delta c_{l,pot}$. Together with a negative $\Delta \dot{c}_{l,pot}$ in the downstroke, ft_2 will be highly negative in the downstroke. To improve this behaviour the forcing term is set to zero for the downstroke. Besides, figures (2) and (3) show that the predicted shedding in the upstroke is larger than in the measurments. Thereto the forcing term is lowered and will be changed to:

$$ft_2 = 0.1k_s\left(-0.08\Delta c_{l,pot} + 1.5\tau\Delta\dot{c}_{l,pot}\right), \tag{20}$$

From figures (1) and (2) it is visible that there are higher frequencies in the downstroke. This is not modelled as cf_{21} is a constant value in the downstroke, see Eq. (9). To allow shedding, the coeffcient is changed to:

$$cf_{21} = \begin{cases} 60\tau k_s\left[-0.01\left(\Delta c_{n,pot} - 0.5\right) + 2(\Delta c_{n2})^2\right] & if\ \dot{\alpha} > 0 \\ 60\tau k_s\left[-0.01\left(\Delta c_{n,pot} - 0.5\right) + 12(\Delta c_{n2})^2\right] & if\ \dot{\alpha} \le 0 \end{cases}, \tag{21}$$

The damping in the downstroke is set higher than in the upstroke.
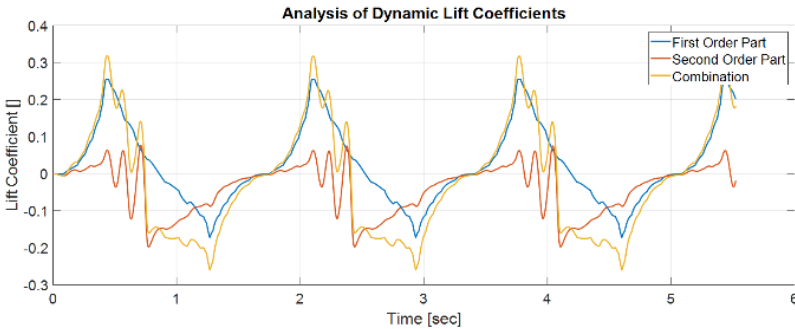

Figure 5: Analysis of the dynamic lift coefficient

9

3.5 Prediction of Vortex Shedding

The shedding frequency will depend on the angle of attack. The current model does not predict a dependency and so it has to be improved in this aspect. The Strouhal number uses the chord or the projected chord perpendicular to the incoming flow. Because the projected chord length is driven by the angle of attack, it is proposed to add the projected chord length to the "spring" term (cf_{20}) of the second order part. This allows for the desired dependency of stiffness. From Eq. (1) it can be inferred that when projecting the chord perpendicular to the incoming flow this is effectively the same as projecting the Strouhal number. The new equation for cf_{20} will now be:

$$cf_{20} = 10 * k_{s,pr}^2 [1 + 3(\Delta c_{l2})^2][1 + 280^2 \tau^2 \dot{\alpha}^2], \tag{22}$$

With:

$$k_{s,pr} = k_s * \sin(\alpha), \tag{23}$$

3.6 Optimization for (Airfoil Specific) Constants

An unconstrained minimization algorithm in MATLAB is used to optimize empirical constants. The algorithm searches for the lowest summation of the absolute errors, from Eq. (13), of all cases considered. The constants selected for this analysis are shown in the initial row of table (2). The constants are selected as are in equations effected by the modifications from this chapter, and also because they have a high influence on the output of the Snel model. Three optimization analyses have been carried out: a global optimization which covers all cases, an optimization which focussed only on the cases with a mean angle of attack of 14 or 20 degrees, and an optimization has been conducted on the low reduced frequency cases. The initial constants as in table (2) are the start values for the optimization. The results for all individual cases, using the error analysis described in section 2.2, are shown in figure (6). It can be seen that the global optimization is the most optimal. The global optimization gives the most consistently lower error compared to the initial model. In Bladed the Beddoes Leishman dynamic stall model has three sensitive constants which are allowed to be changed by the user. For the Snel model, the optimization shows that two constants are the most sensitive. The optimization output showed significantly different values for these constants for the NACA 4415 and the S809 airfoil. They are shown in the improved row of table (2). These constants must be allowed to be changed by users of a turbine design code. The same goes for the Strouhal number. The constants are:

- C1 from table (2). Which will be called the First Order Coefficient
- C2 from table (2). Which will be called the Second Order Forcing Coefficient.

As a result of this optimization step the following changes are implemented. Eq. (6) will change to:

$$cf_{10} = \begin{cases} \frac{1+C_1*\Delta c_{n,pot}}{8(1+60\tau\dot{\alpha})} & if \ \dot{\alpha}c_{n,pot} \leq 0 \\ \frac{1+C_1*\Delta c_{n,pot}}{8(1+80\tau\dot{\alpha})} & if \ \dot{\alpha}c_{n,pot} > 0 \end{cases}, \tag{24}$$

Eq. (20) will change to:

$$235 \quad ft_2 = 0.01k_s\left(-0.04\Delta c_{n,pot} + C_2\tau\dot{\Delta}c_{n,pot}\right), \tag{25}$$

The First Order Coefficient C_1 will be 0.5 for the NACA 4415 airfoil and 0.2 for the S809. For the Second Order Forcing Coefficient C_2 will be 1 and 1.5 respectively. Table 2 shows that for Eq. (18) and Eq. (19) the constants remain the same. Therefore these remain unchanged. Finally Eq. (21) will become as follows:

$$cf_{21} = \begin{cases} 60\tau k_s\left[-0.01\left(\Delta c_{n,pot} - 0.5\right) + 2(\Delta c_{n2})^2\right] & if\ \dot{\alpha} > 0 \\ 60\tau k_s\left[-0.01\left(\Delta c_{n,pot} - 0.5\right) + 14(\Delta c_{n2})^2\right] & if\ \dot{\alpha} \leq 0 \end{cases}, \tag{26}$$

240

|	Equation	(6)	(20)		(22)		(21)	(21) downstroke
	Initial	0.5	0.1	-0.08	1.5	10	280	60	12
Constant	Improved	0.2 ; 0.5 (C1)	0.01	-0.04	1.5 ; 1 (C2)	10	280	60	14

Table 2: Constants used for optimization
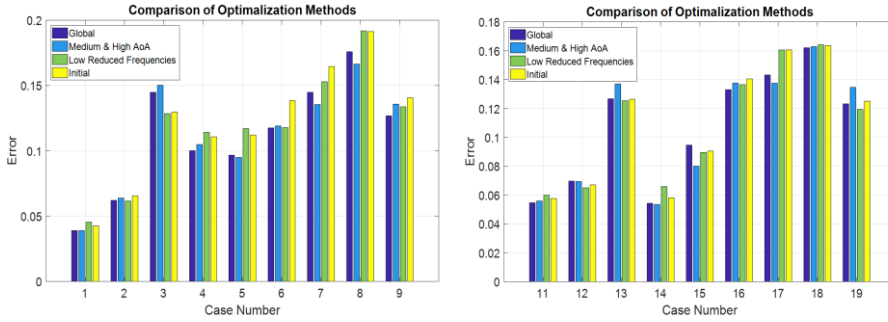
Figure 6: Absolute error analysis of the optimization runs for all cases from table 1.

4. Results of the Proposed Modifications

245 The modified Snel model is implemented as described in chapter 2.1 and tested against the same set of experiments as in table (1). The results of the modified Snel model are shown in figures (7) and (8). In comparison to figures (2) and (3) it is noted that the shedding prediction at low reduced frequency is improved. For the higher reduced frequency the model also captures the shedding slightly better, even though there is less shedding present. Furthermore, it can be seen that the frequency changes between both cases as desired. It is important to investigate the impact changes on different situations and airfoils. Figure (9)
250 displays the updated model in combination with the S809 airfoil. The improved model still predicts slightly lower values than the experiments but the overall trends are followed nicely and shedding frequency matches the experiment well.

11
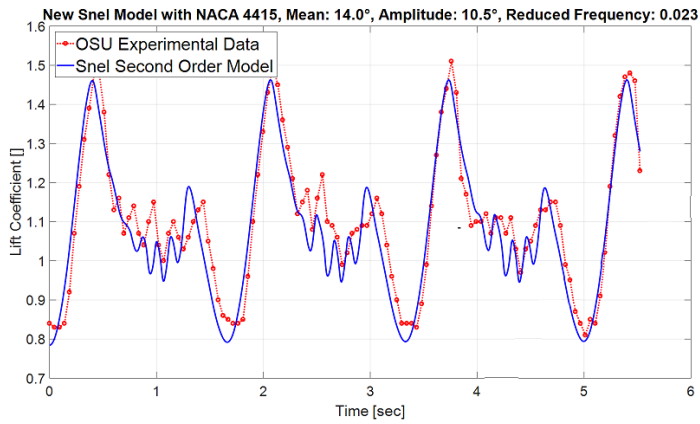
Figure 7: Lift coefficient over time of the improved Snel model (NACA 4415 Airfoil with mean angle of attack of 14°, amplitude of 10.5°, and reduced frequency of 0.023)
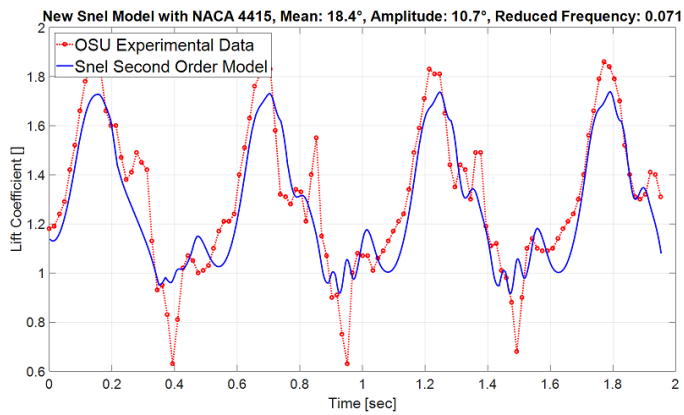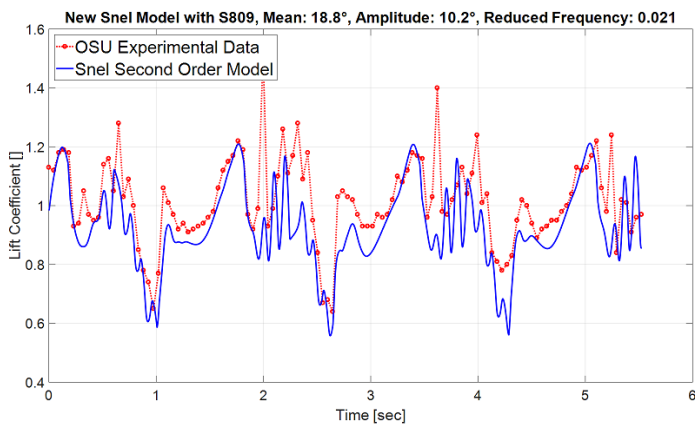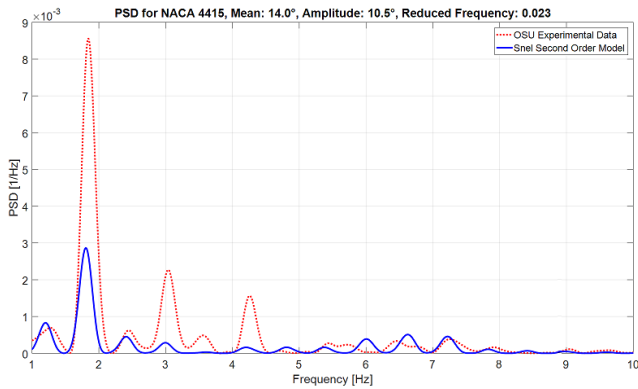

Figure 8: Lift coefficient over time of the improved Snel model (NACA 4415 Airfoil with mean angle of attack of 18.4°, amplitude of 10.7°, and reduced frequency of 0.071)

Figure 9: Lift coefficient over time of the improved Snel model (S809 Airfoil with mean angle of attack of 18.8°, amplitude of 10.2°, and reduced frequency of 0.021)

12

Another goal of the proposed changes to the Snel model was to capture, predict, and match the vortex shedding and the shedding frequency of airfoils in dynamic stall conditions. In order to check the validity of these changes in a quantitative way

265 a frequency domain analysis has been performed. The power spectral density (PSD) estimate is calculated using Welch's method. The Hamming window is set equal to the number of data points and the number of overlapped values to 50% of the window length. The forcing frequency is removed from the plot as the shedding frequencies are higher and the forcing frequency will take up a large proportion of the PSD. The results for both airfoils are shown in figures (10) and (11). From the figures it becomes clear that the Snel model captures, for both airfoils at different mean angles of attack and different reduces

270 frequencies, the self-induced shedding frequencies fairly correct. However, as shown in figures (7)(8) and (9) there is still room for improvement here. All predicted shedding frequencies match frequencies observed in the measurements whereas the intensity isn't always correct. Care must be taken with the higher frequencies as the OSU measurement has a relatively low sampling frequency and might therefore not fully capture some higher frequency dynamics.

275 **Figure 10: Power spectral density of experimental data and the improved Snel model (NACA 4415 Airfoil mean angle of attack of 14°, amplitude of 10.5°, and reduced frequency of 0.023)**
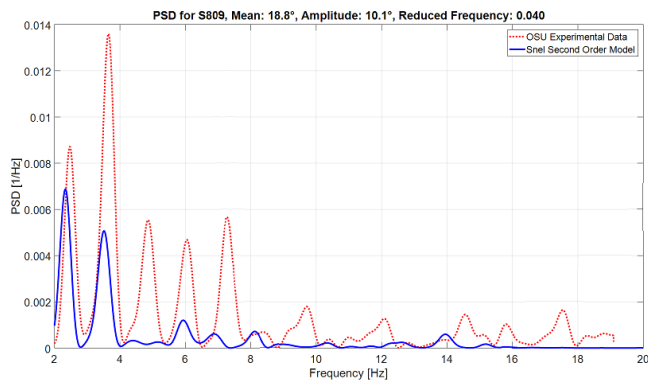

Figure 11: Power spectral density of experimental data and the improved Snel model (S809 Airfoil with mean angle of attack of 18.8°, amplitude of 10.1°, and reduced frequency of 0.040)

13

To quantify the improvements, the effects of all previous changes on the overall absolute error of the new model are shown in figure (12) together with the overall error of the initial of chapter 3. It is seen that the improved model outperforms the initial on almost every case with a single exception. The initial model already gave very accurate results for that case and the increase in error is very small compared to the reduction achieved in all other cases. It is also noted that the overall prediction of the shedding phenomena has been improved. Hence it can be concluded that the model changes developed and presented in this paper improve the performance of the Snel second order model.
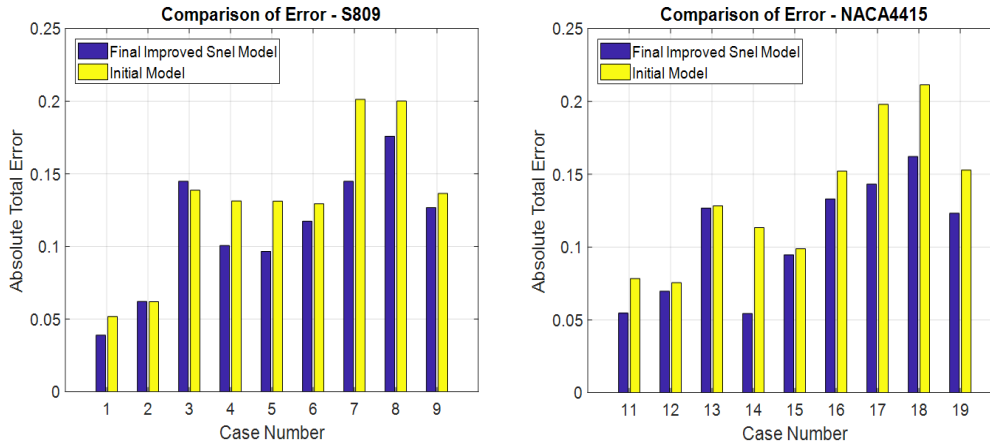

Figure 12: Comparison of the total absolute error of both the initial and improved Snel model

5. The Updated Snel Model Performance with New MEXICO Data

The Model Rotor Experiments In Controlled Conditions (MEXICO) was a project in which an instrumented, 3 bladed turbine of 4.5m rotor diameter was tested (Schepers and Boorsma et al., 2012). The MEXICO experiments were carried out in the Large Scale Low Speed Facility (LLF) of the German Dutch Wind Tunnels (DNW)(Schepers and Boorsma et al., 2012). The blades were fitted with pressure sensors at 25, 35, 60, 82, and 92% radial positions. Tests were performed with 30m/s wind speed, blades pitched to vane, and yaw inflow angles in the range of -90° to 30° and for three azimuthal positions (0°, 120°, and 240°). This data set is particularly valuable for the testing of dynamic stall models as it represents standard load cases set out by the IEC (DNV GL, 2016). For a complete overview of the MEXICO and New MEXICO project reference is made to (Schepers and Boorsma et al., 2012). (Khan, 2018) conducted a similar research with different dynamic stall models and will be used as baseline in this paper. The improved Snel model from this paper will be tested against the New MEXICO data sets of table(3) (β = wind direction, θ = pitch angle) to see if the additions and changes to the model have a positive influence on the accuracy. The blade geometry, mass and flexibility distribution are modelled in Bladed according to New Mexico data. The modal damping in the calculations is set to 0.5%. In the runs the rotational augmentation is turned off just like in (Khan, 2018), also the tip and root loss Prandtl corrections are turned off as well as tower shadow effects. 21 blade stations, as in the geometry description of the New Mexico blade, are used. The starting and ending radius for the dynamic stall model are 25%

and 95%. The normal force distribution in axial flow, with pitch -2.3° and thus an angle of attack about 90°, is given in figure (13). The Snel model shows roughly the same size of normal force fluctuations as in the experiment. (Khan, 2018) found
305 similar deviations in the mean values of the normal force distributions with different turbine design codes and different dynamic stall models. A reason for this deviation is not mentioned and should be part of further research. The improved Snel model predicts shedding at -2.3° pitch with axial flow, due to the addition of the normal force coefficient, while the original model as in (Khan, 2018) does not. The PSD of the time series of both the New Mexico data and the Bladed output are compared. The normal force time series are standardized by subtracting the mean and dividing by the standard deviation. The
310 Hamming window is set to equal the number of data points and the number of overlapped values to 50% of the window length. The results are shown in figure (14) at radial location of 82% of the total span.

Case no.	Case type	Data Point	U [m/s]	β [°]	Θ [°]	Ω [rpm]
1		372	± 30	0	90	0
2		382	± 30	0	75	0
3	Standstill with axial flow	373	± 30	0	45	0
4	(rough)	386	± 30	0	30	0
5		400	± 30	0	12	0
6		375	± 30	0	-2.3	0
7		405, 406, 407	± 30	-90	90	0
8		408, 409, 410	± 30	-60	90	0
9	Standstill with yawed flow	411, 412, 413	± 30	-45	90	0
10	(rough)	414, 415, 416	± 30	-30	90	0
11		420, 421, 422	± 30	15	90	0
12		423, 424, 425	± 30	30	90	0

Table 3: Investigated Cases from the New MEXICO Experiments

The updated Snel model shows significantly higher frequency vibrations in the normal force of the New Mexico blade.
315 Figure(15) shows the normal force distribution for the blade at azimuth 120° for the yawed case with 30° wind direction and 90° pitch. Interesting to notice for this case is that the angle of attack will be negative. The Snel model does not show any unsteadiness in the normal force distribution. Further research is needed to explain and improve the Snel model for negative angles of attack.

15
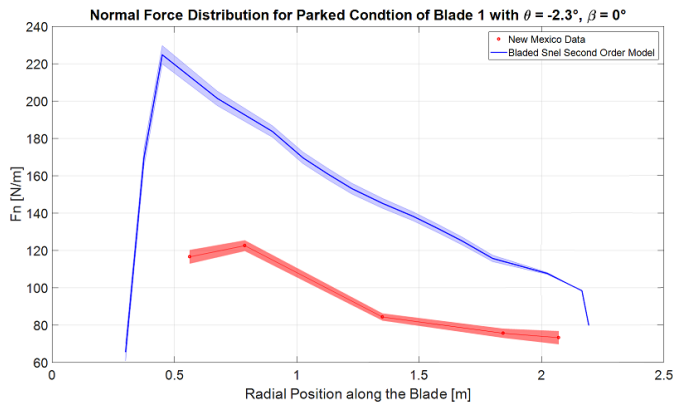
Figure 13: Normal force distribution of the blade at 0° azimuth with -2.3° pitch and 0° wind direction. The bold line represents the mean value and the shaded area is the standard deviation.
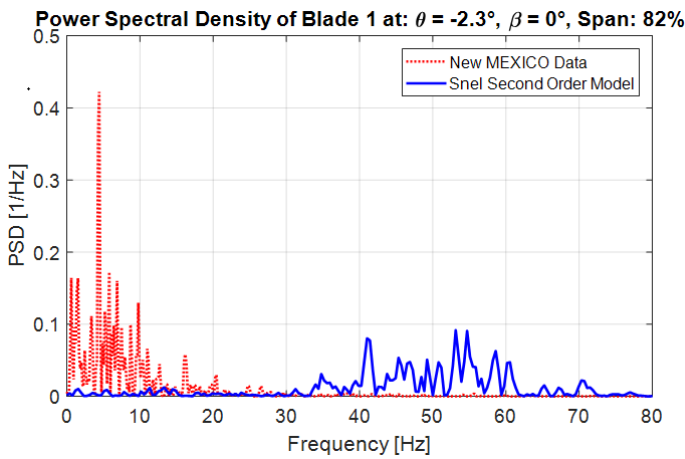
Figure 14: Power spectral density at 82% span of the blade at 0° azimuth with -2.3° pitch and 0° wind direction.

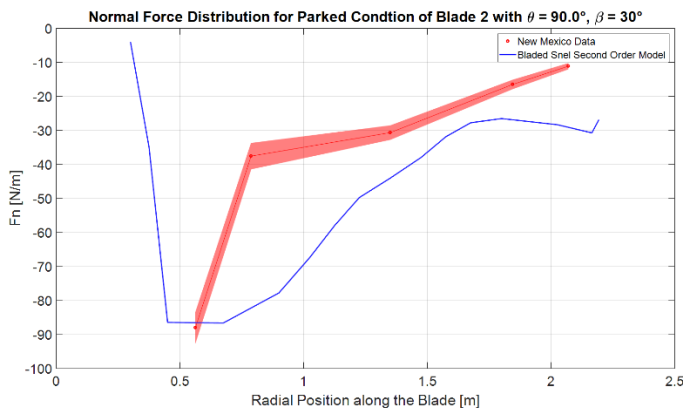**Figure 15: Normal force distribution of the blade at 120° azimuth with 90° pitch and 30° wind direction. The bold line represents the mean value and the shaded area the standard deviation.**

330 A single reason for the higher frequency prediction has not been found. Several possibilities are suggested: First: the modal damping is not specified in the New Mexico turbine data and was therefore assumed as 0.5%. Second: The impact of different airfoils from the New Mexico blade is unknown. The First Order or Second Order Forcing Coefficients might require other values. Furthermore, the Strouhal number for the New Mexico blade is not 0.2Hz at high angles of attack (Khan, 2018). Research by (Skrypinski et al. 2014 and Zou et al. 2015) shows that for airfoils with an effective angle of attack of around 90

335 degrees the Strouhal number should be more around 0.10-0.13Hz. This ought to be implemented in the model and tested in further research. Third: wind tunnel effects are not modelled in Bladed. The wind field in bladed has zero turbulence and wind tunnel effects. More research the Snel model in Bladed with actual turbine data is advised.

6. Conclusion and Recommendations

The Snel model has been validated with OSU experimental data and following this validation propositions for improvements

340 have been made. The improvements to the model have been tested and lead to a reduction in the overall error between the Snel model and the OSU experimental data. Furthermore, an improvement in the prediction of both the amplitude and frequency of vibrations in the measurements has been accomplished. The improved model is implemented in Bladed turbine design software and tested against the New Mexico experimental data. Prediction of normal force distributions along the blade seems to match earlier implementations in other turbine design codes while the mean value of the normal force is not correct. This is a major

345 area for further research and improvement. The Snel model predicts the amplitude of the normal force vibrations well while the predicted frequency is higher than in the experiment. A single reason for this has not been found and therefore further research is advised into the Snel model. (Truong, 2017) proposed a similar modification of his original model as (Snel, 1997) and therefore also similar to the model adaptations presented in this paper. The main difference lies in the incorporation of the steady lift data as described in chapter 2. The authors highly recommend a study comparing both the model described in

350 (Truong, 2017) and the model presented in this paper. The model as proposed is formulated on the basis of variations in angles of attack. It is recommended for further research to delve into the possibility to adept this model to dynamic variation in inflow velocity for the case of rotating and vibrating blades.

The proposed Snel second order dynamic stall model might become a valuable addition to the modelling of dynamic behaviour in stall conditions. As the conditions tested in this paper are often design driving, the Snel model looks promising for more

355 accurate prediction of design driving (fatigue and extreme) loads and more cost efficient wind turbine designs.

Code/Data Availability

The paper uses the publicly available OSU oscillating airfoil experiments data. The implementation of the Snel model in this paper (and the final improved model) in the MATLAB environment is available and can be requested from the corresponding author.

Author Contributions

J.G. Schepers has been the thesis supervisor within the MSc. Program, he has been involved in writing (reviewing and editing) of the final thesis and corresponding paper.

M. Kloosterman was thesis supervisor from DNV GL and contributed to the implementation of the model in the MATLAB environment and furthermore, M. Kloosterman has been a part of the investigation, validation, and improvement of the model as well as implementation of the model in the Bladed turbine design software. Finally he has been reviewing and editing the final thesis and corresponding paper.

Competing Interests

The authors declare that they have no conflict of interest.

References

Choudry, A. et al.: An insight into the dynamic stall lift characteristics. J. Exp. Thermal and Fluid Science, 58, 188-208, doi:10.1016/j.expthermflusci.2014.07.00, 2014

De Vaal, J.B.: Heuristic modelling of dynamic stall for wind turbines, MSc. Thesis, TU Delft, 2009

DNV GL: Loads and site conditions for wind turbines, Standard DNVGL-ST-0437, 2016

Gonzalez A. and Munduate X.: Unsteady modelling of the oscillating S809 aerofoil and NREL phase VI parked blade using the Beddoes-Leishman dynamic stall model., Journal of Physics: Conference Series 75 (1), 2007

Hoffmann, M.J. et al.: Effects of Grit Roughness and Pitch Oscillations on the NACA 4415 Airfoil, Technical Report NREL/TP-422-7815, https://wind.nrel.gov/airfoils/OSU_data/reports/3x5/n4415.pdf, 1996

Hollierhoek J.G. et al.: Comparing different dynamic stall models., Wind Energy, 16, 139-158, doi:10.1002/we.548, 2013

Khan, M.A.: Dynamic Stall Modelling for Wind Turbines, MSc. Thesis, TU Delft, uuid:f1ee9368-ca44-47ca-abe2-b816f64a564f, 2018

Leishman, J.G.: Challenges in modelling the unsteady aerodynamics of wind turbines, J. Wind Energy, 5, 82-132, doi:10.1002/we.62, 2002

Madsen, M. H. Aa., Zahle, F., Sørensen, N. N., and Martins, J. R. R. A.: Multipoint high-fidelity CFD-based aerodynamic
390 shape optimization of a 10 MW wind turbine, Wind Energ. Sci., 4, 163–192, https://doi.org/10.5194/wes-4-163-2019, 2019

McCroskey W.J.: The Phenomenon of Dynamic Stall.: Technical Report NASA-TM-81264, https://ntrs.nasa.gov/search.jsp?R=19810011501, 1981

Montgomerie, B.: Dynamic Stall Model Called "Simple", Technical Report ECN-C--95-060, 1996.

Pellegrino, A. and Meskell, C.: Vortex shedding from a wind turbine blade at high angles of attack, J. Wind Eng. Ind. Aerodyn.,
395 121, 131-137, doi:10.1016/j.jweia.2013.08.002, 2013

Riziotis, V.A. et al.: Stability analysis of parked wind turbine blades using a vortex model, Conference Science of making torque from the wind, Heraklion, Greece, 2010.

Schepers J.G. and Snel H.: Model Experiments in controlled conditions, Technical Report ECN-E-07-042, Petten, The Netherlands, 2007.

400 Schepers, J.G. and Boorsma, K. et al.: Final report of IEA Task 29, Mexnext (phase 1), Report ECN-E—12-004, 2012

Schreck, S. et al.: HAWT Dynamic Stall Response Asymmetries under Yawed Flow Conditions, J. Wind Energy, 3, 215-232, doi:10.1002/we.40, 2000

Schrek, S.: The NREL Full-Scale Wind Tunnel Experiment, J. Wind Energy, 5, 77-84, doi:10.1002/we.72, 2002.

Skrzypinski W, Gaunaa M, Sørensen N, Zahle F, Heinz J.: Vortex induced vibrations of a DU96-W-180 airfoil at 90 deg angle
405 of attack, J. Wind Energy 17: 1495–1514. DOI: 10.1002/we.1647, 2014

Snel. H.: Heuristic modelling of dynamic stall characteristics, European Wind Energy Conference, Dublin Castle, Ireland, 429-433, 1997.

Sørensen N. et al.: CFD computations of the second round of MEXICO rotor measurements, J. Phys.: Conf. Ser. 753 022054, 2016

410 Truong, V.K.: A 2-D dynamic stall model based on a HOPF bifuctation, 19th European Rotorcraft Forum Proceedings, C23, Cernobbio, Italy, 1993.

Truong V.K.: Modeling Aerodynamics, Including Dynamic Stall, for Comprehensive Anaylsis of Helicopter Rotors, Aerospace,4, 21, doi:10.3390/aerospace402021, 2017

Wala A.A.S. et al.,: A Beddoes-Leishman – type model with an optimization-based methodology and airfoil shape parameters,
415 Wind Energy, 21, 590-603, doi:10.1002/we.2180, 2018

Zou, F., Riziotis, V.A., Voutsinas, S.G, Wang, J.: Analysis of vortex and stall induced vibrations at standstill conditions using a free wake aerodynamic code,. J Wind Energy, Vol. 18, Issue 12, pp 2145-2169, 2015